

Article

Effect of Reaction Time and Hydrothermal Treatment Time on the Textural Properties of SBA-15 Synthesized Using Sodium Silicate as a Silica Source and Its Efficiency for Reducing Tobacco Smoke Toxicity

Nerea Juárez-Serrano ^{*}, Desiré Berenguer, Isabel Martínez-Castellanos, Inmaculada Blasco, Maribel Beltrán and Antonio Marcilla 

Chemical Engineering Department, University of Alicante, Apartado 99, 03690 Alicante, Spain; desi.bm@ua.es (D.B.); i.martinez@ua.es (I.M.-C.); inma.blasco@ua.es (I.B.); maribel.beltran@ua.es (M.B.); antonio.marcilla@ua.es (A.M.)

* Correspondence: nerea.juarez@ua.es

Abstract: The synthesis of SBA-15 has been optimized using sodium silicate, an inexpensive precursor of SBA-15. In this work, the influence of synthesis times of the precipitation and the hydrothermal treatment steps, on the textural properties developed as well as for reducing the toxic compounds generated in tobacco smoking, has been studied. The hydrothermal treatment has been proved to be necessary to obtain materials with adequate performance in this particular application. Twenty-four hours of hydrothermal treatment provide materials with the best properties. Although the reaction stage usually involves the mixing of reagents during 24 h, 40 min is enough to obtain a material with stick-like morphology and typical textural properties. Moreover, between 1 and 2 h of reaction time, the material proved to have the best performance for the purpose of reducing the toxicity of the products generated during the tobacco smoking process. These results are of great significance for an eventual scaling up to industrial scale of the SBA-15 manufacturing process. Results of a pilot plant experiment in a batch of 4 kg of SBA-15 are reported.

Keywords: SBA-15; hydrothermal treatment time; synthesis; reaction time; tobacco toxicity reduction



Citation: Juárez-Serrano, N.; Berenguer, D.; Martínez-Castellanos, I.; Blasco, I.; Beltrán, M.; Marcilla, A. Effect of Reaction Time and Hydrothermal Treatment Time on the Textural Properties of SBA-15 Synthesized Using Sodium Silicate as a Silica Source and Its Efficiency for Reducing Tobacco Smoke Toxicity. *Catalysts* **2021**, *11*, 808. <https://doi.org/10.3390/catal11070808>

Academic Editors: Roman Dziembaj and Lucjan Chmielarz

Received: 27 May 2021
Accepted: 28 June 2021
Published: 30 June 2021

Publisher's Note: MDPI stays neutral with regard to jurisdictional claims in published maps and institutional affiliations.



Copyright: © 2021 by the authors. Licensee MDPI, Basel, Switzerland. This article is an open access article distributed under the terms and conditions of the Creative Commons Attribution (CC BY) license (<https://creativecommons.org/licenses/by/4.0/>).

1. Introduction

According to the IUPAC, mesoporous materials present pores in the range of 2–50 nm. Such pores can have different shapes such as spherical, cylindrical, platelets, sticks or fibers, and can be arranged in varying structures [1]. In 1992, a new family of ordered mesoporous materials was synthesized by Mobil Corporation laboratories [2] including MCM-41, with hexagonally ordered cylindrical pores, and MCM-48 with cubic pore structure. These materials are characterized by having an ordered porous system with a narrow distribution of diameters, high surface area and pore volume. In 1998, Zhao et al. [3,4] developed a new mesoporous siliceous material with a hexagonal structure. This material was named Santa Barbara Amorphous (SBA)-15 where 15 is a number corresponding to a specific pore structure and surfactant (hexagonally ordered cylindrical pores synthesized with a specific the surfactant).

The synthesis of this mesoporous material occurs through a sol–gel process called liquid crystal templating (LCT) [5], where the structures can be formed by the interaction of organic template molecules (surfactant) and inorganic species (silica source). The surfactant used is Pluronic P123, a triblock copolymer of poly(ethylene oxide) and poly(propylene oxide), in aqueous solution. When the concentration of the surfactant in solution reaches a threshold value, called micellar critical concentration, the molecules form aggregates (micelles). Then the micelles are grouped forming supramicellar structures, which vary depending on the concentration and temperature. In general, at moderate temperatures,

the cylindrical micelles are grouped first forming a hexagonal phase, which evolves into a cubic (isotropic) phase, and subsequently to a lamellar structure as the concentration of the surfactant increases [6]. Then, the silica molecules present in the aqueous solution condense around the micelles and a solid of sticky morphology is obtained, which contains a high amount of surfactant occluded. When the formation of SBA-15 is finished, the temperature is increased for the hydrothermal treatment, and the polyethylene oxide chains of the surfactant become more hydrophobic, resulting in an increased pore size and reduced microporosity and surface area [7]. Finally, the surfactant is removed, usually by calcination in air at elevated temperatures, giving rise to a material with the final porous structure.

During all these synthesis processes and due to the interactions with the surfactant, micropores are generated and distributed perpendicular to the hexagonal channels, penetrating the silica walls. This dual porosity gives SBA-15 differential characteristics, which have made it a very useful material in various applications, among which it stands out as adsorbents or catalysts [8–12]. In this sense, the SBA-15 is a very versatile material that presents a great variety of synthesis routes and applications. For example, Nguyen et al. [13] synthesized it from brick ash. Synthesizing the material with ZnO/SBA-15, they obtained certain properties that allowed methylene blue to photodegrade. On the other hand, Niculescu et al. [14] used SBA-15 to produce metal oxide species capable of promoting the oxidation of alkenes with H₂O₂. This mechanism falls into the group of green chemistry, since it only produces water as a by-product. Furthermore, the structure of silica also favors access to bulky compounds.

Many authors have studied the effect of different variables in the synthesis of SBA-15. For example, the variation of the silica source [15–17] and its ratio to the surfactants [18,19], the time and temperature of the hydrothermal treatment [15,20–22], the pH [23], calcination temperature [24,25] and the temperature of the reaction stage [17,21]. Fulvio et al. [15] studied the effect of time and temperature of the hydrothermal treatment using two silica sources (TEOS and sodium metasilicate), observing a decrease in surface area when both variables were increased. In addition, the volume of mesopores and pore diameter showed an increasing tendency. SBA-15 is typically obtained in the form of sticks but modifying variables such as acidity, agitation rate and temperature, this material can be synthesized in the form of platelets, spheres or rods [15,16,22,26,27].

Kosuge et al. [26] reported a very simple SBA-15 synthesis yielding a material with very interesting textural properties without applying the hydrothermal treatment, which is a usual stage in the synthesis of this type of mesoporous materials [15,17]. This process modification would be very interesting for reducing the cost of large-scale production of the SBA-15.

Great research efforts have been focused on the addition of various materials on tobacco with the aim of reducing the number of toxic compounds in smoke. In this sense, some mesoporous materials have been studied as elements capable of retaining some of these compounds [28–34].

The use of these types of materials (i.e., MCM-48, MCM-41, SBA-15) and zeolites (i.e., NaA, NaY, HUSY, ZSM-5, H β), in the filter or directly mixed with tobacco to reduce the toxicity of the tobacco smoke, has been described elsewhere [35–37]. Our research group has studied the use of MCM-41, SBA-15 and zeolites (HUSY, HZSM-5 and H β) to reduce the yields of toxic compounds in tobacco smoke and we have reported that the addition of these materials to tobacco allows the reduction of most of the compounds present in the mainstream of tobacco smoke [28,38–40]. In these works, the effect of these meso and microporous materials (having their particular properties) were studied. Nevertheless, to our knowledge, the study of the effect of the textural properties of a given material on its behavior for reducing the toxicants of tobacco smoke when mixed with tobacco has not been attempted. In addition, SBA-15 is the material that has presented the best characteristics for this application, showing good reduction percentages and better stability.

In previous works [41,42], we have reported the effect of different variables such as temperature, time or stirring rate at different steps of the synthesis using TEOS as a

precursor. The objective of the present work was to synthesize SBA-15 materials using sodium silicate as silica source (an easier handling and lower cost reactant as compared to TEOS) at different hydrothermal treatment and reaction times. This study has been developed in order to provide more insight on the effect of the SBA-15 synthesis conditions on its effect as a tobacco toxicant reducer. In this case, to maximize the possibilities of reducing the manufacturing costs, we have focused on short times. On the other hand, scaling up of the SBA-15 production process is rarely considered in literature and very few studies comment on it and report results of such trials. Moreover, the scaling up attempts reported batches of tens of grams [43,44]. Thus, another objective of the present work was running a scaling up experiment in a pilot plant scale of a batch of around 4 kg of SBA-15, making it possible to check the viability of the process at the industrial scale.

2. Results and Discussion

2.1. Study of Hydrothermal Treatment Time

2.1.1. SBA-15 Characterization

Figure 1 shows SEM images of samples obtained at different hydrothermal treatment times. As can be seen, when no hydrothermal treatment was applied (H0), the material shows thicker and not well-formed sticks. Moreover, when the time of hydrothermal treatment increases, well-formed sticks are formed with increased size and length, yielding larger particles.

The nitrogen adsorption isotherms at 77 K for the four samples are shown in Figure 2. All samples present a type IV isotherm, according the IUPAC classification, with a hysteresis loop at a relative pressure of 0.6–0.8, which is characteristic of the mesoporous materials with cylindrical channels in a hexagonal arrangement [20,22]. All samples present an H1 type hysteresis cycle, typical of solids with a narrow distribution of uniform mesopores. Moreover, the shape of the desorption branch of the isotherm indicates that most of the mesopores are emptied at a single relative pressure, what is characteristic of materials with ink-bottle pores [45,46]. When no hydrothermal treatment was applied (H0), the material presents a lower hysteresis loop that moves to lower values of P/P_0 which would reveal a loss of properties. When the hydrothermal treatment time increases, the hysteresis loop increases, with the curves of the samples prepared at 6 and 15 h being very similar (H6 and H15 in Table 1) and the H24 sample showing a significant increase in the hysteresis cycle, indicating an improvement of the adsorption properties.

Table 1. Textural properties of the samples synthesized.

Sample	Reaction Time (h)	HT Time (h)	S_{BET}^a (m ² /g)	V_t^b (cm ³ /g)	V_{micro}^c (cm ³ /g)	V_{meso}^* (cm ³ /g)	ρ_a^d (g/cm ³)	PD ^e (nm)	a_0^f (nm)
H0	24	0	793	0.771	0.324	0.447	0.099	4.9	11.0
H6	24	6	735	0.641	0.210	0.431	0.058	6.0	11.7
H15	24	15	728	0.664	0.202	0.462	0.055	6.0	12.7
H24	24	24	799	0.790	0.228	0.562	0.043	6.2	13.1
R1/3	0.3	24	735	0.609	0.289	0.320	0.281	3.8	12.1
R2/3	0.6	24	980	1.010	0.392	0.618	0.062	6.1	12.7
R1	1	24	946	0.957	0.373	0.584	0.061	6.1	12.9
R2	2	24	970	1.120	0.381	0.739	0.057	6.2	13.1
R4	4	24	834	0.962	0.327	0.635	0.053	6.1	13.1
R6	6	24	791	0.920	0.313	0.607	0.053	6.0	13.1
R24 (H24)	24	24	799	0.790	0.228	0.562	0.043	6.2	13.1

^a BET surface area; ^b total pore volume at $P/P_0 = 0.995$; ^c Dubinin micropore volume; ^{*} $V_t - V_{\text{micro}}$; ^d apparent density; ^e pore diameter BJH method applied to the desorption branch; ^f length of the hexagonal unit cell.

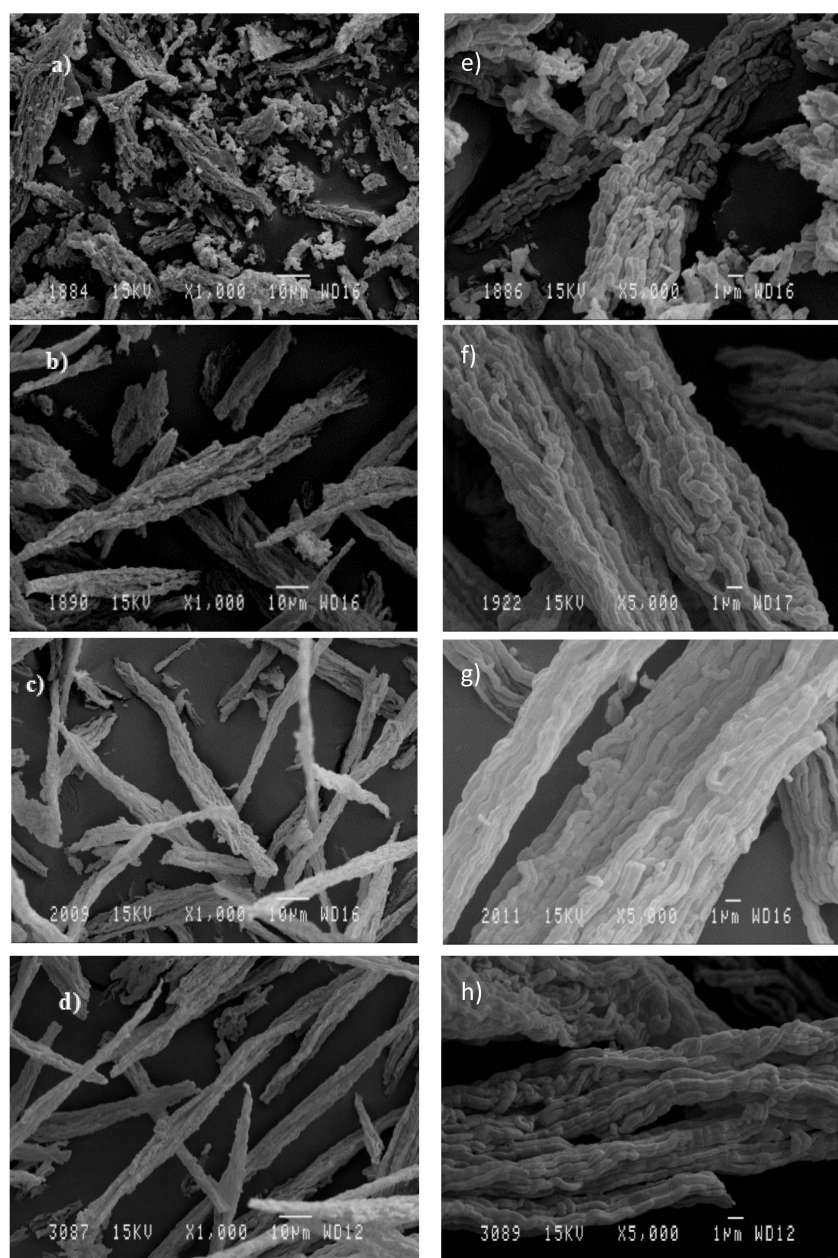


Figure 1. SEM images of the samples prepared at different hydrothermal treatment times and magnifications: (a,e) H0, (b,f) H6, (c,g) H15 and (d,h) H24.

Table 1 shows the textural properties derived from the isotherms, i.e., BET surface area, external surface area, specific pore volume and average pore size. As can be observed, the samples prepared at intermediate hydrothermal treatment times (H6 and H15) have similar properties, and an increase of all the properties is observed for the sample prepared after 24 h (H24). As expected, the sample without treatment (H0) has the lowest pore size (4.9 nm) since the hydrothermal treatment promotes the PEO chains to become more hydrophobic, resulting in pore widening [7]. Consequently, not applying such treatment would not allow this process to occur. Table 1 also shows the apparent density that is related to the morphology of the particles and to the mode in which they can be dispersed on the strands of the tobacco. This parameter has been used by other authors such as Nagata et al. [47] to characterize a similar material such as MCM-41. As can be observed, the apparent density decreases when increasing the hydrothermal time, affecting the performance of this material in the application studied here, as will be shown.

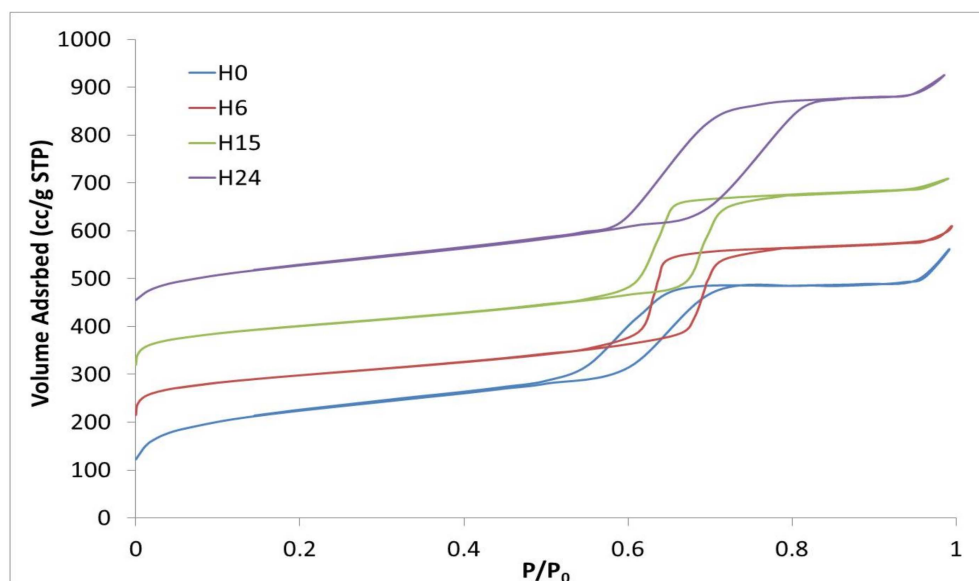


Figure 2. 77K N_2 adsorption isotherms of the samples prepared at different hydrothermal treatment times (samples H6, H15 and H24 are offset vertically by 100, 200 and 300 cm^3/g STP, respectively).

Figure 3 shows the XRD patterns of the samples obtained at different hydrothermal treatment times (H0, H6, H15 and H24). The spectra show the three characteristic peaks of the diffraction planes (100), (110) and (200) of the 2-d hexagonal space group $p6mm$ of the SBA-15 [3,20]. The definition and position of these peaks is related to the mesoporous hexagonal symmetry, i.e., lower values indicating a more ordered structure [17,48,49]. The relative position of the peak of the plane (100) of sample H0 is shifted to higher values of 2θ , while the peak (110) practically does not appear and the (200) peak moves to higher values, indicating a poorly organized structure. When the hydrothermal treatment time increases, all planes move to lower values of 2θ and the intensity and definition of (110) and (200) peaks increase, showing that more ordered materials can be obtained when increasing the time of this stage. In addition, from the relative position of the peak of the plane (100), it is possible to obtain the d-spacing, while the peaks (110) and (200) are related to the 2D hexagonal reorganization of the pores [50]. For the calculation of the unit cell parameter, a_0 was obtained as $a_0 = \lambda / (\sqrt{3} \sin \theta)$. The unit cell parameter increases when the time of hydrothermal treatment increases reaching a maximum value of 13.1 nm for sample H24 (Table 1). Sample H0, where hydrothermal treatment was not applied, shows a value of unit cell parameter of 11.0 nm. Therefore, we can conclude that the hydrothermal treatment time, as expected, is closely related to the structural stability of the resulting material.

Figure 4 shows the relation of the textural properties and apparent density with the time of hydrothermal treatment. Three different tendencies can be observed in Table 1. BET area (S_{BET}) and the total pore volume (V_t) are shown in Figure 4a as a function of the hydrothermal treatment time (V_{meso} and V_{micro} show the same tendency) and present convex behavior with minimum values at intermediate hydrothermal treatment times. On the other hand, the apparent density (Figure 4b) shows an almost linear decreasing behavior. Finally, the pore size and the unit cell present an increasing behavior up to stable values after 15 h of treatment (see Table 1).

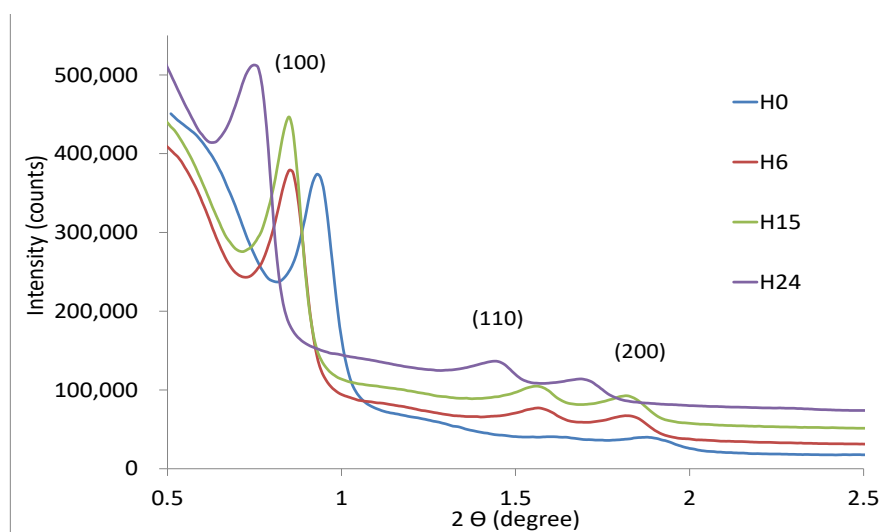


Figure 3. XRD spectra of the samples prepared at different hydrothermal treatment times (samples H6, H15 and H24 are offset vertically by 20,000, 40,000 and 60,000 counts, respectively).

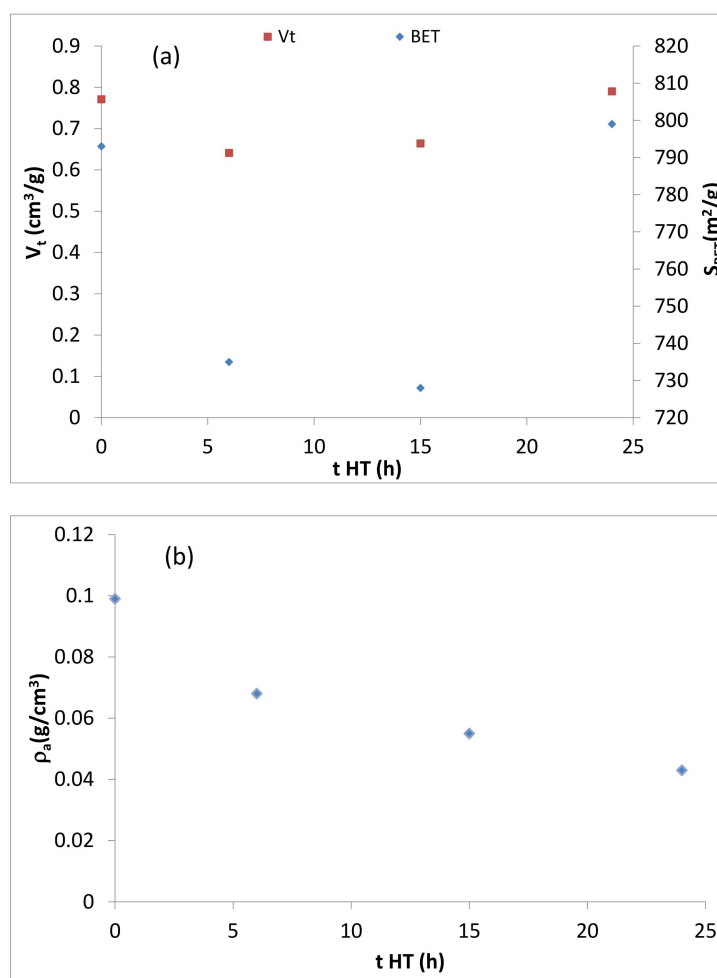


Figure 4. Variation with the hydrothermal treatment time (tHT) of: (a) total volume (V_t) and BET area (S_{BET}) and (b) apparent density ρ_a .

2.1.2. Products Generated during the Smoking Process

Table 2 shows the reductions (i.e., the amount of a compound obtained when smoking 3R4F tobacco without a catalyst minus the corresponding amount obtained when smoking tobacco mixed with a catalyst, divided by the amount obtained when smoking 3R4F tobacco without a catalyst, expressed as %) obtained in total particulate material (TPM), nicotine and CO for the different materials synthesized. As can be seen, when the material is not subjected to hydrothermal treatment (H0), poor results are obtained. This material only reduces 13.5% in TPM and 18.4% in nicotine. Moreover, H0 does not reduce the formation of CO, contrarily its yield was increased. When time of hydrothermal treatment increases an increase in the effective reduction of TPM, nicotine and CO is observed, reaching TPM reductions higher than 60% in the case of sample H24. Taking into consideration these results (Table 2), we can conclude that to obtain high reductions in the products evolved in tobacco smoking, it is necessary to apply the hydrothermal treatment and that the higher the duration of this stage, the better the reductions in TPM, nicotine and CO.

Table 2. Yield reductions obtained in the smoking process for the different catalysts studied.

Sample	% R _{TPM}	% R _{Nicotine}	% R _{CO}
H0	13.5	18.4	−25.2
H6	32.5	19.2	8.8
H15	48.3	39.5	24.1
H24	62.3	50.5	23.3
R1/3	10.9	22.0	6.8
R2/3	60.1	63.5	16.5
R1	69.6	75.5	36.4
R2	74.6	75.7	37.7
R4	69.3	69.3	36.6
R6	61.9	61.6	26.1
R24 (H24)	62.3	50.5	23.3

Figure 5a shows the reductions of TPM, nicotine and CO vs. the time of hydrothermal treatment, where a linear increasing trend can be observed for TPM and nicotine, while CO remains almost constant from 15 h of treatment on. Figure 5b shows the reductions in nicotine, tar and CO vs. V_t , (plots, not shown, vs. V_{meso} and V_{micro} show similar trends). As can be seen, this graph shows an apparently abnormal behavior for the sample H0 (i.e., that with $V_t = 0.771 \text{ cm}^3/\text{g}$). Nevertheless, this sample has a very high apparent density (Figure 5c) and a poorly developed mesopore structure, though other textural parameters are relatively high. Additionally, the micrographs of this sample show different morphology of the particles as compared to the rest of the samples (Figure 1). Consequently, this catalyst would involve a poorer contact with the tobacco, thus explaining the poor reductions observed, despite the high pore volume. These facts are in good agreement with the “straw spreading” mechanism described by Wei Gang Lin et al. [37]. According to these authors, the apparent density is related to the ability of the material to spread on the tobacco fibers, and showing the importance of considering the apparent density and morphology in the performance of this type of catalyst in smoking applications. Moreover, reductions in nicotine, tar and CO show a linear decreasing behavior with apparent density, showing again the clear correlation with this variable (Figure 5c). Nevertheless, this variable alone cannot explain the behavior of these catalysts in this application, as will be shown when studying the influence of the reaction time.

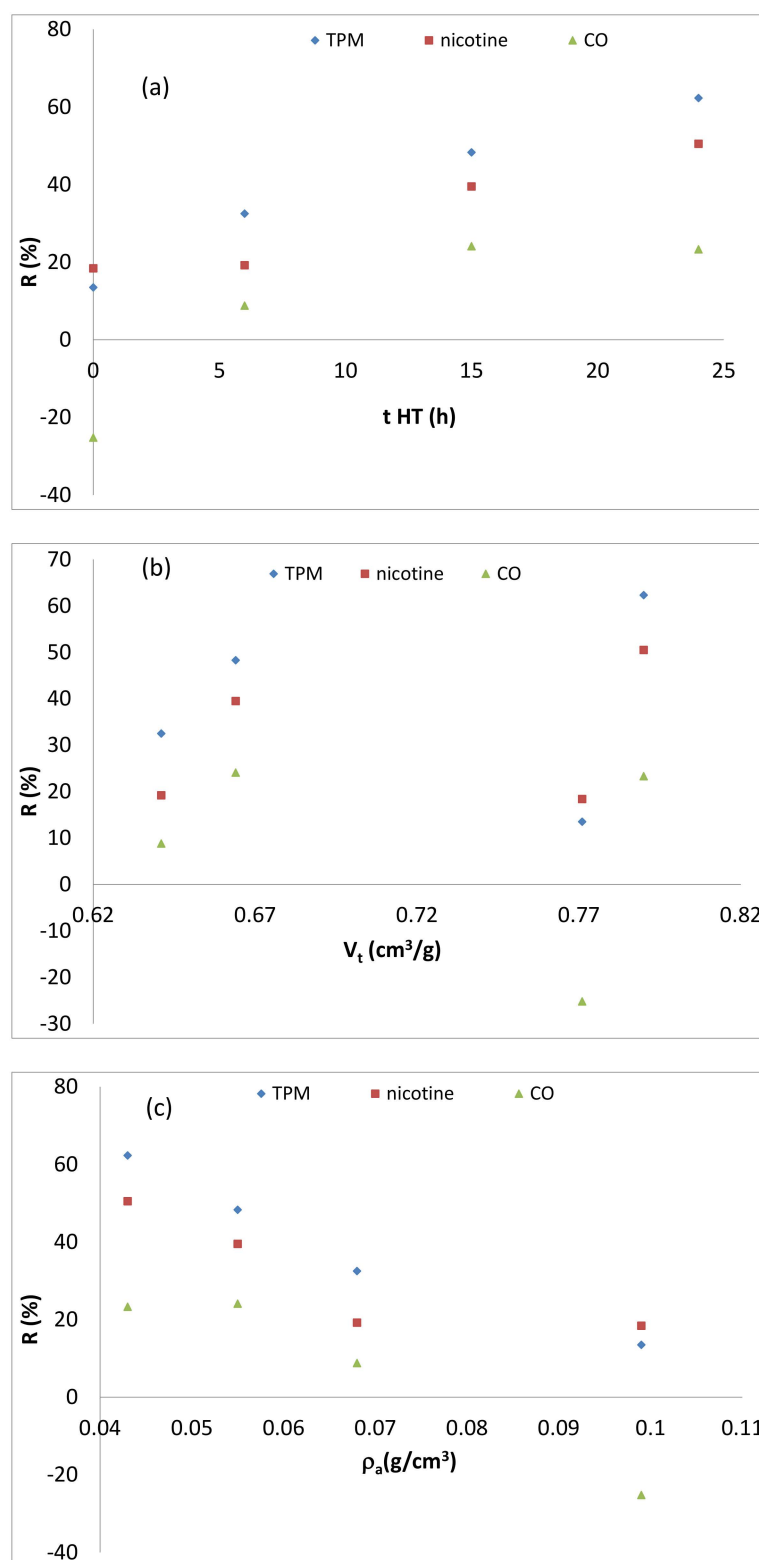


Figure 5. Reduction (R) of TPM, nicotine and CO yields vs.: (a) hydrothermal treatment time (tHT), (b) total pore volume V_t and (c) apparent density ρ_a .

Table 3 shows the reductions determined for the compounds analyzed and identified in the gas fraction. Sample H0 shows many compounds increasing their yields. Only important reductions in the formation of acetonitrile can be observed. When the time of

hydrothermal treatment increases, the reduction is higher. Several compounds, such as toluene, present reductions larger than 80% with 15 and 24 h of treatment (H15 and H24).

Table 3. Yield reductions obtained in the gas fraction for the different catalysts studied.

Compound	Family	% Reduction									
		H0	H6	H15	H24(R24)	R1/3	R2/3	R1	R2	R4	R6
Methane	Paraffins	-16.5	14.3	23.6	15.3	-25.2	-10.0	20.9	18.7	15.8	9.3
Ethane	Paraffins	-13.7	21.8	22.6	17.6	-25.4	-9.9	15.8	14.5	11.9	1.2
Ethylene	Olefins	-23.4	18.7	24.5	26.5	-24.2	-13.1	16.2	16.5	15.8	8.6
Ethyne	Others	-50.6	15.8	25.8	21.9	-29.9	-29.9	2.0	21.9	9.7	-2.2
Propane	Paraffins	-12.8	21.3	22.4	28.1	-26.0	-11.9	11.6	12.4	10.4	2.2
Propene	Others	-22.9	23.3	21.7	29	-24.3	-10.0	14.1	14.2	14.2	13.2
Iso-butane	Paraffins	-86.5	61.5	14.5	38.7	-67.3	-1.5	-3.2	13.3	-3.5	-6.8
Chloromethane	Others	-13.1	22.4	14.9	27.2	-18.3	-2.7	18.2	19.0	17.9	-7.3
Butane	Paraffins	-23.1	24.9	17.8	26	-21.5	-6.0	2.6	8.3	3.6	-8.4
1-Butene	Olefins	-11.5	26.4	25.0	11.3	-35.4	-7.7	5.0	12.1	7.2	1.8
1,2-Propadiene	Olefins	-8.1	21.0	28.6	30.4	-34.7	-0.5	-2.3	27.7	12.9	7.5
1,3-Butadiene	Olefins	-8.2	13.9	17.0	20	-22.7	-8.8	17.5	16.5	12.6	7.2
Isobutene	Olefins	-25.0	26.8	19.3	21.9	-26.2	-14.5	7.3	10.0	10.5	8.7
cis-2-Butene	Olefins	-11.5	28.4	23.9	21.5	-26.0	-6.8	11.6	16.0	16.5	12.8
Pentane	Paraffins	2.8	39.5	14.7	38	-17.0	-6.0	12.7	10.1	15.0	-3.3
Methanethiol	Others	-43.0	-47.5	-19.4	-21.2	-17.8	6.2	63.4	41.3	37.6	18.3
Hydrogen cyanide	Others	1.1	15.0	14.1	34.7	-27.7	-23.9	-10.5	3.8	6.9	-6.1
1-Pentene	Olefins	0.6	23.1	12.6	30.6	-42.2	-13.8	8.9	4.6	8.4	-6.6
Furan	Aromatics	-2.6	-54.7	15.6	34	-7.5	5.0	25.0	25.1	15.0	14.1
Isoprene	Olefins	-48.6	-10.8	17.3	17.8	-36.5	-44.9	-4.1	6.1	17.4	5.5
Hexane	Paraffins	22.8	34.2	29.5	-6.2	-78.0	-87.2	4.9	-9.3	32.4	26
1-Hexene	Olefins	-14.4	23.4	17.9	23.8	-13.1	-2.6	24.6	24.8	29.0	-3.3
Benzene	Aromatics	-5.8	25.0	19.3	27.6	-25.0	4.2	40.3	40.9	35.1	22.1
Acetaldehyde	Aldehydes	-9.9	23.9	39.1	34.3	-6.9	1.8	36.5	29.1	26.8	-5.9
Acrolein	Aldehydes	-96.2	-34.4	-6.4	-20.9	-46.0	-63.8	7.6	-20.9	-11.8	-61.9
Propionaldehyde	Aldehydes	17.2	27.8	14.6	21.7	-23.8	-5.1	39.1	36.0	31.6	13.3
Acetonitrile	Others	43.1	-55.8	-13.0	-6.4	8.7	42.4	84.7	77.6	72.8	57.3
Toluene	Aromatics	13.1	86.6	81.2	83.5	-3.8	16.0	52.3	45.6	39.9	11.4
Crotonaldehyde	Aldehydes	15.5	27.3	-73.3	-48.2	2.0	20.0	24.5	72.3	66.3	39.9
Isobutyraldehyde	Aldehydes	-19.9	-47.7	45.5	9.9	-9.3	-0.3	29.3	34.3	18.0	-4.7
Total Reductions (%)		-19.9	18.1	23.2	23.5	-24.1	-10.8	22.4	19.9	17.9	13.6

To facilitate the analysis, the different compounds have been grouped by their functional groups into five families, i.e., paraffins, olefins, aromatics, aldehydes and “others”. As can be seen in Figure 6, the sample with no hydrothermal treatment (H0) only presents low reductions in aromatic compounds and the rest of the families have negative reductions (i.e., yields higher than those obtained when smoking tobacco). When the time of treatment is low (H6), no reductions were observed in aldehydes and “others” families and when the time increases, higher reductions in all the families appear, being the sample H24 the best one in all the families with the exception of the aldehydes group, that presents a somewhat smaller reduction than the H15 sample.

Table 4 shows the reductions of the compounds obtained in the condensed fraction. Again, the sample with no hydrothermal treatment (H0) presents the worst results and as in the case of the gases, many compounds were generated in larger proportion than in the case of tobacco with no catalyst (negative reductions). This effect is especially remarkable in the case of hydroquinone, N-propyl-nornicotine, limonene and farnesol, which are very favored. When the time of hydrothermal treatment increases, large reductions can be observed with sample H24 being the one that presents the highest reductions. It should also be noted that at low hydrothermal treatment time (H6) several compounds, as in the case of the sample H0, present no reductions, as for example cotinine, farnesol and hexadecanoic acid-ethyl ester. In addition, many compounds are not detected as a result of the hydrothermal treatment, as is the case of phenol, o-cresol, 1H-Indole, hydroquinone and N-propyl-nornicotine (this compound only disappearing for the H24 sample).

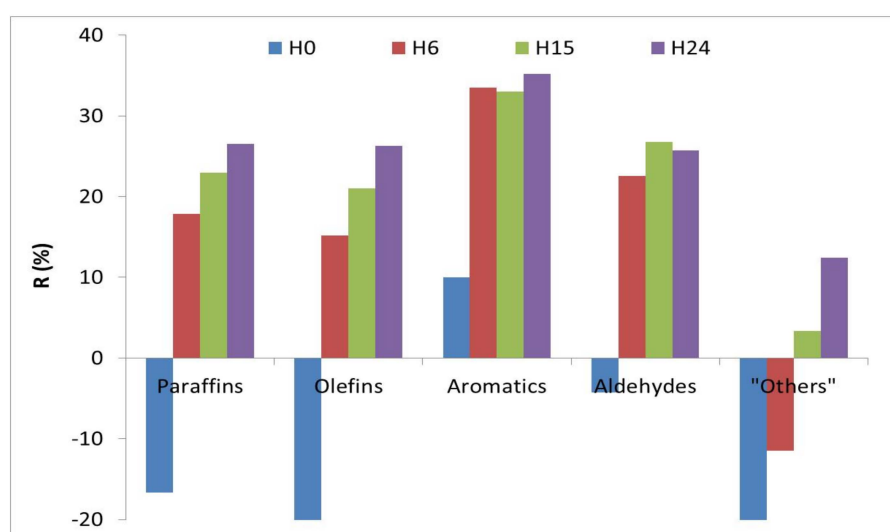


Figure 6. Reductions of the groups of compounds considered in the gas fraction vs. hydrothermal treatment time.

Table 4. Yield reductions obtained in the condensed fraction for the different catalysts studied.

Compound	Family	% Reduction									
		H0	H6	H15	H24(R24)	R1/3	R2/3	R1	R2	R4	R6
Ethanol, 2-(1-methylethoxy)-	Epoxy	40.91	18.2	35.5	45.4	-2.73	49.91	59.9	72.77	73.34	88.36
Styrene	Aromatic	-18.02	100	100	100	56.3	64.56	69.88	71.58	66.96	31.3
2-Cyclopenten-1-one, 2-methyl-	Carbonylic	85.26	72.1	100	100	65.46	78.39	89.47	83.01	77	47.22
Phenol	Phenolic	44.13	100	100	100	-10.75	44.24	53.72	27.16	27.32	23.34
Limonene	Others	-91.08	100	77.6	88.4	-19.72	67.58	66.09	66.74	53.62	79.31
2,3-Dimethyl-2-cyclopenten-1-one	Carbonylic	55.34	18.2	57.3	47.3	15.42	21.84	47.67	81.31	72.51	62.79
o-Cresol	Phenolic	35.5	100	100	100	24.31	95.38	95.98	91.46	86.17	87.23
p-Cresol	Phenolic	31.05	29.8	49.9	68.5	13.33	77.29	88.4	87.74	83.02	61.11
Phenol, 2-methoxy-	Phenolic	10.01	100	100	100	22.89	85.14	94.8	77.59	76.94	84.3
3-Ethyl-2-hydroxy-2-cyclopenten-1-one	Carbonylic	-68.32	100	100	100	42.26	85.1	85.86	94.1	94.7	89.76
2,3-Dihydro-3,5-dihydroxy-6-methyl-4H-pyran-4-one	Carbonylic	15.2	57.3	71.6	61.6	35.77	78.39	86.53	86.4	78.23	67.73
Phenol, 2,4-dimethyl-	Phenolic	-16.09	100	100	100	43.35	88.81	98.38	90.7	91.57	72.45
Phenol, 4-ethyl-	Phenolic	8.66	41.4	82	93.3	47.2	81.09	90.14	92.05	74.99	77.07
Naphthalene	PAH	42.81	53.7	57.9	64.7	72.73	69.55	64.76	63.85	61.98	76.28
Ethanone, 1-(3-methylphenyl)-	Carbonylic	57.73	47.6	56.8	6.9	74.82	93.08	92.43	82.35	79.9	75.89
p-cresol 2 methoxy	Phenolic	-79.95	100	48.8	80.8	28.29	66.36	54.46	79.13	67.18	77.65
2,3-Dihydro-benzofuran	Epoxy	-31.54	100	100	100	48.31	82.11	95.07	72.56	46.76	64.46
Hydroquinone	Phenolic	-99.38	100	100	100	15.94	40.99	41.65	39.92	27.32	33.31
1H-Indole	Nitrogenous	92.29	100	100	100	28.65	58.4	74.31	82.24	67.04	44.9
4-vinyl-2-methoxy-phenol	Phenolic	-56.18	44.4	61.1	81.9	1.57	70.16	79.49	77.12	57.78	68.03
Nicotine	Nitrogenous	18.49	19.2	39.5	50.5	22.19	63.61	75.8	75.99	69.77	61.79
1H-Indole, 3-methyl-	Nitrogenous	50.54	100	100	100	12.7	65.96	71.59	82.31	64.31	75.29
Myosmine	Nitrogenous	23.89	26.1	29.7	27.5	25.4	74.95	78.3	85.23	78.74	76.09
Phenol, 2-methoxy-4-(2-propenyl)-	Phenolic	29.51	100	6.6	60.3	13.27	63.13	89.85	61.26	49.3	76.04
Nicotyrine	Nitrogenous	-80.61	100	56.8	90.3	51.42	77.11	83.6	86.02	80.51	77.82
Norsolanadiona	Carbonylic	-32.29	100	65.6	84.2	20.72	63.76	80.9	74.34	73.29	81.78
2,3-Binitrogenous	Nitrogenous	17.7	-18.3	40	49.8	25.23	94.88	94.03	89.62	93.54	79.49
Megastigmatrienone	Carbonylic	-0.13	100	72	85.7	21.78	77.74	82.41	77.05	68.3	47.97
N-propyl- nornicotine	Nitrogenous	-98.01	100	87.9	96.9	9.79	33.37	35.67	55.81	42.02	38.27
Cotinine	Nitrogenous	18.27	-25.1	33.9	100	22.96	55.03	75.81	78.15	64.46	66.9
5-Tetradecene	Aliphatic	8.49	-10.1	24	66.3	19.6	55.82	75.75	82.18	63.51	62.75
N(b)-formylornicotine	Nitrogenous	23.58	100	44.6	88.7	8.95	64.12	80.64	80.62	73.99	72.1
NEOPHYTADIENE	Aliphatic	-1.03	9.4	28.5	75.4	6.11	42.97	60.11	65.57	47.01	57.36
Farnesol	Others	-96.15	-30.9	36.3	43	15.35	61.09	62.99	73.59	58.8	56.82
Hexadecanoic acid, ethyl ester	Carbonylic	-0.81	-36	40.8	50	14.78	14.1	1.41	9.27	2.88	8.54
2,6,10,14,18,22-Tetracosahexaene, 2,6,10,15,19,23-hexamethyl-	Aliphatic	-22.62	100	37.5	74.4	1.57	38.41	54.53	63.15	46.43	47.6
Heptacosane	Aliphatic	-47.39	-23.7	25.3	31.5	30.2	57.41	68.03	76.22	67.09	60.5
Triacontane	Aliphatic	-45.8	-11.7	35.3	32.3	47.07	76.54	77.98	85.2	66.53	67.18
Octadecane	Aliphatic	-12.46	58	79.4	60.8	18.89	61.05	70.18	79.12	80.64	75.96
Tocopherol	Phenolic	-25.34	-23.6	-24.5	26	25.72	75.34	70.96	83.25	73.25	80.44

The compounds analyzed in Table 4 were grouped in six families, nitrogenous (where nicotine was excluded, since it is the major organic compound and has been discussed separately), carbonyls, epoxies, phenols, aliphatics and “others”. The corresponding reductions are shown in Figure 7. When no treatment was applied, no reductions are observed in phenolics, aliphatics and “others” families and low reductions in nitrogenous and carbonyl families were observed. At low times (H6), no reductions were observed in aliphatics and “others” families. When the time of hydrothermal treatment increases, high reductions were observed in all the families, obtaining the largest reductions after 24 h of treatment (H24) although very similar to those obtained in the case of sample H15 for carbonyls, phenols, aliphatics and others.

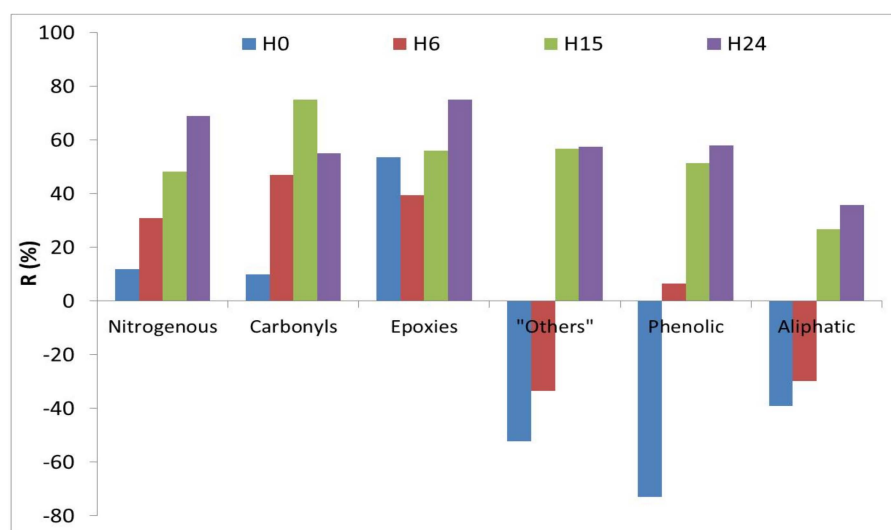


Figure 7. Reductions of the groups of compounds considered in the condensed fraction vs. hydrothermal treatment time.

2.2. Study of Reaction Time

2.2.1. SBA-15 Characterization

For this study, the hydrothermal time was set at 24 h since it was the material that showed the best reductions (H24) and the reaction times studied were 20 min (1/3 h), 40 min (2/3 h), 1, 2, 4, 6 and 24 h (samples R1/3, R2/3, R1, R4, R6, R24). Note that the sample R24 is the same as H24 as indicated in Table 1. Figure 8 shows images obtained by SEM of the different samples obtained at different reaction times. As can be seen, when the time of reaction is low, R1/3, no sticks can be observed. After 40 min (R2/3), short sticks appear, and after 2 h (R2) the resulting material shows long sticks. If the mixing time is increased up to 4 h (R4), the sticks obtained are longer and wider, more similar to those obtained after 6 and 24 h (R6 and R24). The analyses of the images obtained by SEM permits determining that reaction times longer than 2 h yield SBA-15 materials with long stick morphology that become bigger at longer reaction times.

The nitrogen adsorption isotherms at 77 K are shown in Figure 9. All samples present the typical type IV isotherm, with an H1 hysteresis loop at a relative pressure of 0.6–0.8, characteristic of the mesoporous materials. All isotherms show similar curves, with the exception of R1/3 which shows an isotherm with a low and wide hysteresis loop with a two-step desorption branch. This behavior was analyzed by Van Der Voort et al. [51], who concluded that the adsorption–desorption behavior is consistent with a structure comprising both open (first desorption step) and blocked (second desorption step) cylindrical mesopores, which indicates the presence of disordered pore structures. The textural properties of the samples are shown in Table 1. As can be observed, the sample R1/3 has the lowest values of BET area, total pore volume and micropore volume, while samples R2/3, R1, R2, R4, R6 and R24 have similar values without a clear trend. In addition, these samples

have a pore diameter between 6.0 and 6.2 nm, but R1/3 sample presents much narrower pores of only 3.8 nm, showing again that this sample presents lower structural development. Apparent density decreases with increasing reaction times, as observed in the study of the hydrothermal treatment time. The sample R1/3 presents a very high apparent density far out of the trend observed for the rest of the samples. All these data confirm that such a short reaction time is not enough to obtain a material with well-developed properties.

The XDR spectra of these samples (Figure 10) show the three characteristic peaks of the diffraction planes (100), (110) and (200). The position of the peaks of the three planes are very similar for all of them. Nevertheless, in the case of samples R1/3 and R2/3, the peak (100) is not resolved clearly. When the reaction time increases, the peak (100) moves slightly to lower values of 2θ and the peaks of planes (110) and (200) appear better defined and move to lower values of 2θ . Thus, it seems that by increasing the reaction time, a more ordered mesoporous material is obtained. The unit cell parameter, calculated with the position of plane (100), is shown in Table 1, and increases with the reaction time, reaching an identical value for the R2, R4, R6 and R24 samples.

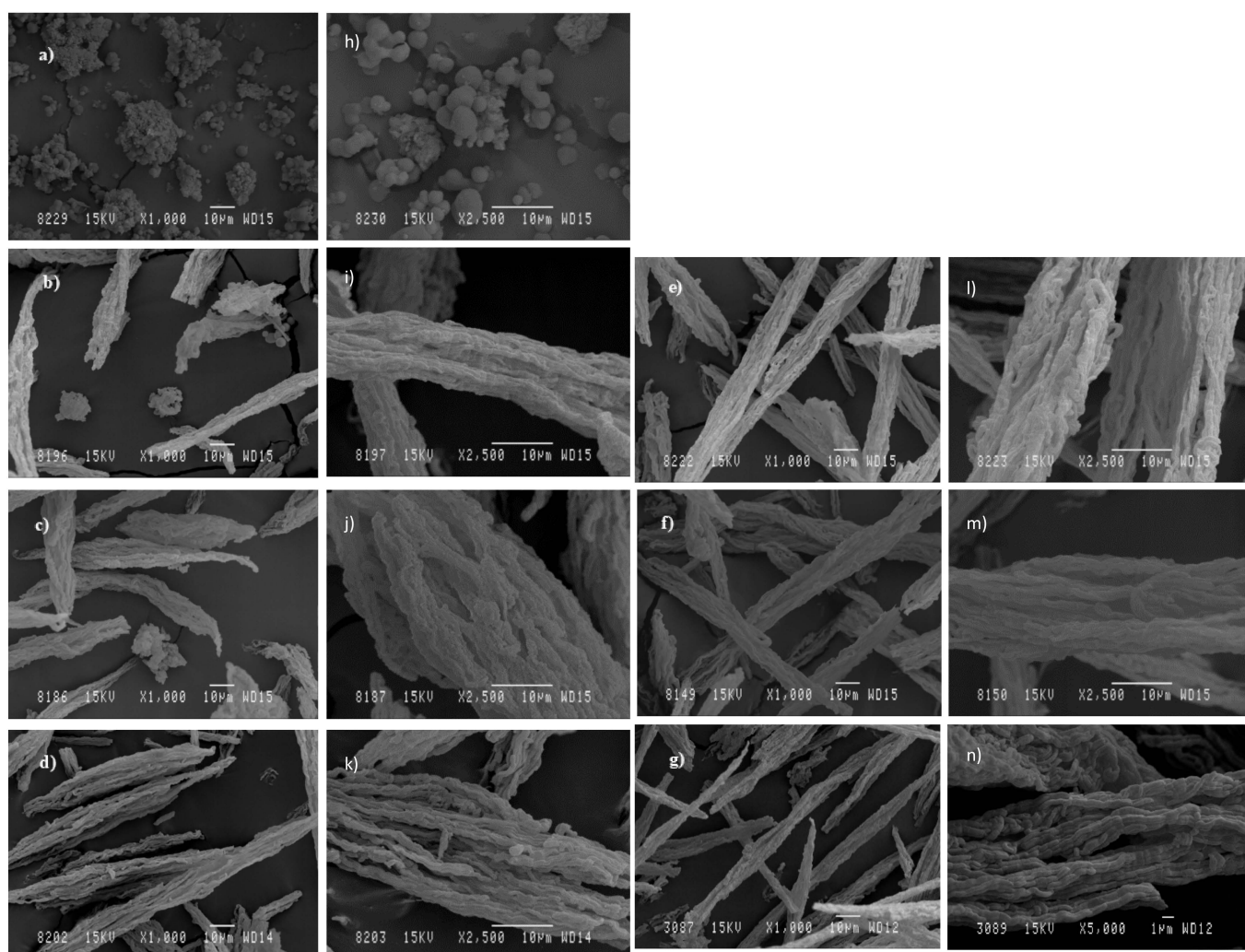


Figure 8. SEM images of the samples prepared at different reaction times and magnifications: (a,h) R1/3, (b,i) R2/3, (c,j) R1, (d,k) R2, (e,l) R4, (f,m) R6 and (g,n) R24 (Figure 1d,h H24).

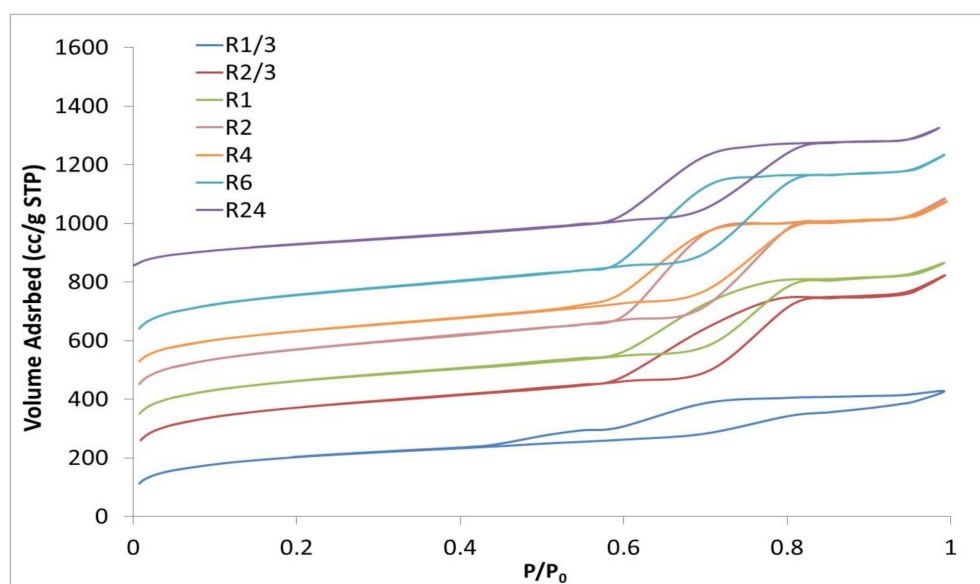


Figure 9. 77K N_2 isotherms of the samples prepared at different reaction times (samples R2/3, R1, R2, R4, R6 and R24 are offset vertically by 100, 200, 300, 400, 500 and 600 cm^3 / STP , respectively).

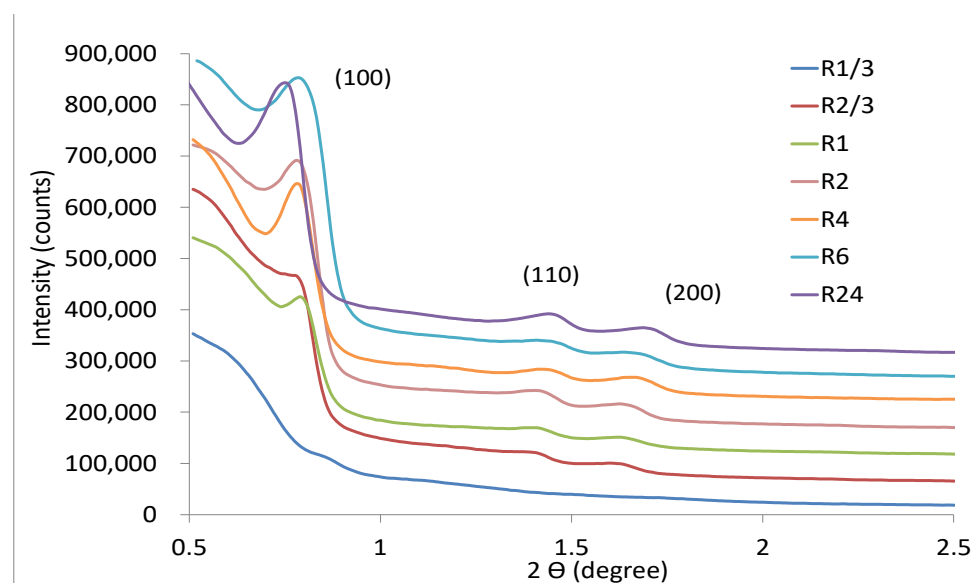


Figure 10. XRD spectra of the samples prepared at different reaction times (samples R2/3, R1, R2, R4, R6 and R24 are offset vertically by 50,000, 100,000, 150,000, 250,000 and 300,000 counts, respectively).

Figure 11 shows the relation between the reaction time with the textural properties and the apparent density. Again, three different tendencies can be observed in Table 1. BET area and the total pore volume (micropore and mesopore volume show the same tendency) show an increasing trend until a maximum at 1 h of reaction and then decrease reaching a constant value (Figure 11a). The apparent density presents an exceptional high value at 20 min of reaction time and then decreases slightly with the reaction time until a stable value is reached at 24 h, being this decrease more moderate than that observed in the study of hydrothermal treatment time (Figures 4b and 11b). Finally, the pore size and the unit cell parameter (Table 1) grows rapidly and stabilizes after short reaction time (2 h).

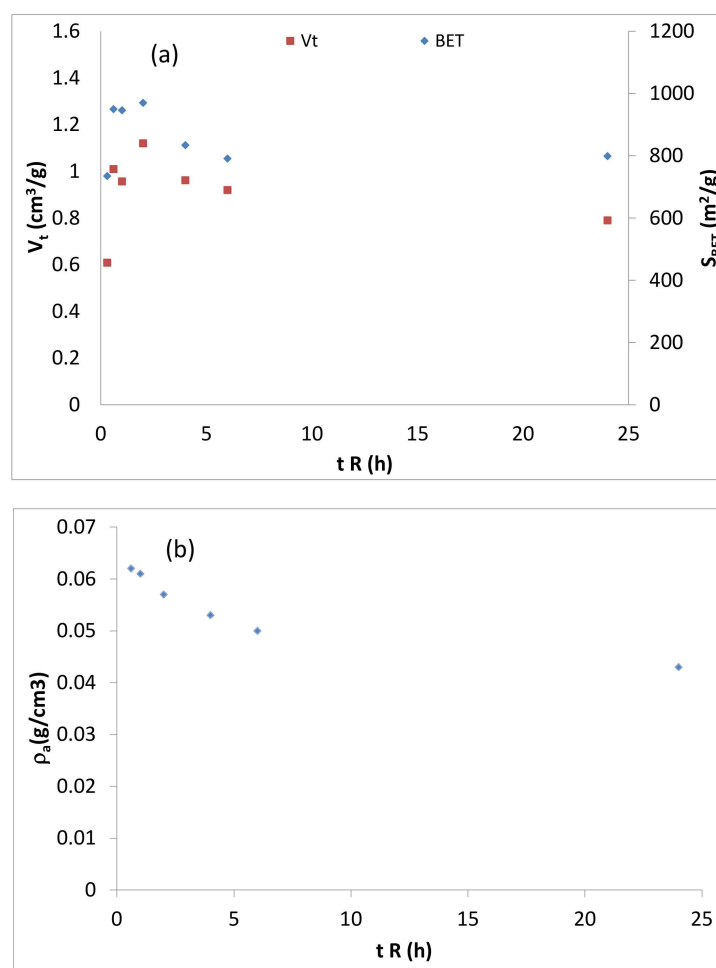


Figure 11. Variation with the reaction time of: (a) total volume (V_t) and BET area (S_{BET}) and (b) apparent density ρ_a .

2.2.2. Products Generated during the Smoking Process

Table 2 and Figure 12a show the reductions obtained in total particulate material (TPM), nicotine and CO vs. the reaction time. As can be seen, the reductions in TPM increase with the time of reaction up to the sample R2 and then decrease slightly. The reduction observed in nicotine follows a similar trend as TPM, thus increasing with increasing reaction time and reaching a maximum at 2 h, although sample R1 shows practically the same value of reduction then sample R2 (see Table 2). When the time of reaction is higher than 2 h, the reductions obtained in nicotine slightly decrease. In addition, the reduction in CO shows the same behavior, but the samples R1, R2 and R4 show similar values. At higher reaction times R6 and R24, the reduction in CO decreases.

Figure 12b shows the reductions in TPM, nicotine and CO yields vs. the BET area. All the textural properties show a very similar behavior as BET area, except the apparent density that shows a slight decrease after 20 min of reaction. The variation of the reductions with respect to the textural properties shows a positive correlation with a certain degree of dispersion. Thus, it can be concluded that the time of reaction produces a maximum both in the development of the textural properties of the synthesized material and in the corresponding behavior in the tobacco smoking application, and that there is a positive correlation between such behavior and the developed textural properties. In this case, the apparent densities of all samples are similar and this property seems not to be so dependent on the reaction time as it is on the hydrothermal treatment time. Consequently, the effect of this property on the smoking application is less marked than in the previous series.

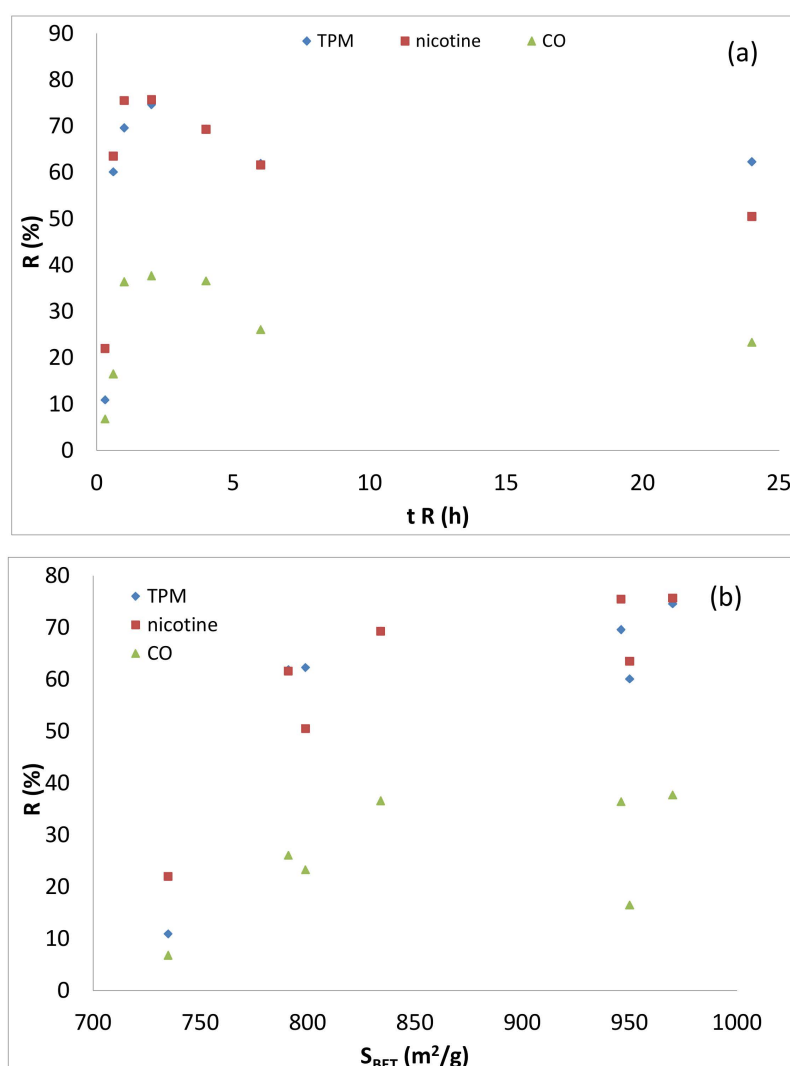


Figure 12. Influence of (a) reaction time and (b) BET area on the reductions of TPM, nicotine and CO.

Table 3 shows the reductions in the compounds analyzed in the gas fraction. As can be seen, samples present a similar tendency to that shown in Table 2. The reduction in the total gases increases with the reaction time until a maximum is obtained. However, the material that shows the greatest reduction in the total gases is R24 but with values very similar to R1. As can be seen, at low reaction times, only low reductions in acetonitrile and crotonaldehyde can be observed. Acetonitrile presents reductions higher than 70% for all samples except R1/3 and R1/6, with a reduction of 85% for the R1 sample. Other compounds that present important reductions are crotonaldehyde, toluene and methanethiol.

The reductions obtained for the functional families analyzed in the gas fraction for samples R1/3-R24 are shown in Figure 13. The principal reductions generated in the gaseous fraction are in aromatics and aldehydes families, and in minor proportion for paraffins and olefins. Figure 13 shows that at low reaction times (R1/3 and R2/3) no reductions are observed for either family, rather increasing the yields of most of the families. When the reaction time increases, the reductions in all the families increase and provoke a maximum in the reductions of all functional groups normally at R1, with the exception of the olefins, that present the maximum for the R24 sample.

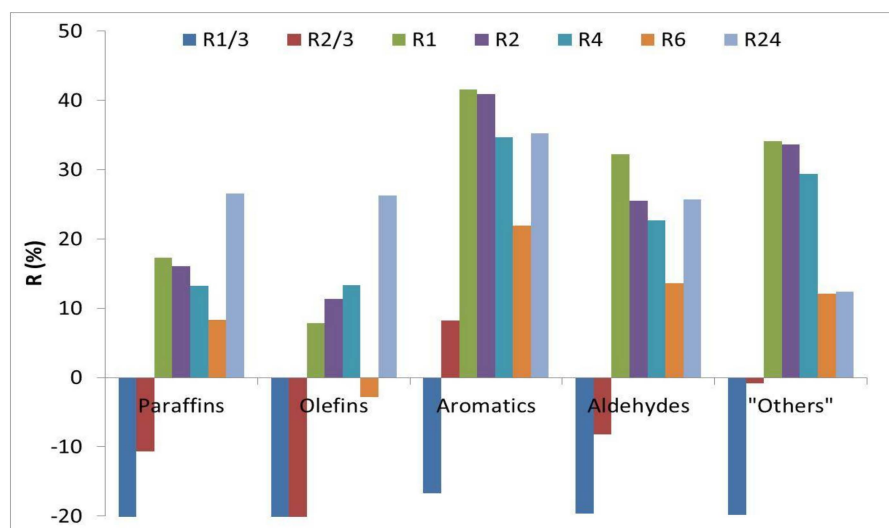


Figure 13. Reductions of the groups of compounds considered in the gas fraction vs. reaction time.

Table 4 shows the reductions obtained for the compounds retained in the condensed fraction. As can be seen, the presence of all the materials provokes the reduction, in different proportion, of the vast majority of compounds. As in the gaseous fraction, the reduction of the compounds of condensed fraction increases when the time of the reaction stage increases, until reaching a maximum, normally located between the samples R2 and R4, and then slightly decreases to increase again at 24 h of reaction time. Many compounds are not detected as is the case of 3-ethyl-2-hydroxy-2-cyclopenten-1-one, phenol 2,4-dimethyl, 2,3-bipyridine and phenol 4-ethyl. In contrast, other compounds such as hexadecanoic acid and ethyl ester show smaller reductions and only present good reduction at high reaction times.

The compounds analyzed in Table 4 were grouped by their functional group. The corresponding reductions are shown in Figure 14. As can be observed, all samples synthesized, regardless of the time of reaction, present important reductions for all the families reaching reductions higher than 80% for the nitrogenous and epoxies families. As in the case of the gas fraction, a maximum in reductions is observed at reaction times of 1–2 h, but in this case all samples lead to positive reductions.

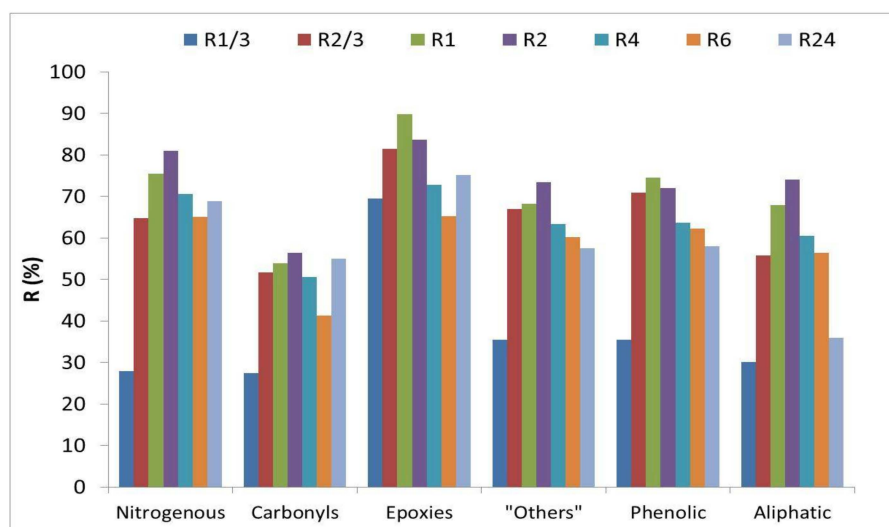


Figure 14. Reductions of the groups of compounds considered in the condensed fraction vs. reaction time.

2.3. Scaling Up Process

This section shows the results obtained with SBA-15 synthesized at the 4 kg pilot plant scale. Table 5 contains the structural properties and the main characteristics of the resulting tobacco smoke obtained including this SBA-15 in the tobacco cigarette (TPM, CO₂ and CO).

Table 5. Structural properties of the sample synthesized in the scaling process and reductions for TPM, CO and CO₂ obtained in the smoking experiment carried out.

Sample	SBET (m ² /g)	Vt (cm ³ /g)	Vm (cm ³ /g)	DP (nm)	ρ _a (g/cm ³)	a ₀ (nm)	TPM (%)	CO ₂ (%)	CO (%)
Scaling	532	0.677	0.207	5.6	0.072	11.2	41.9	8.4	6.3

The textural analysis of the samples highlights some differences with respect to the materials synthesized at the laboratory scale. It could be observed a slight decrease in all the parameters calculated from this sample with respect to the samples synthesized at laboratory scale. Moreover, it seems that the modifications on time at the hydrothermal treatment have greater influence on the variation of these parameters. The stick morphology of the materials was as expected, as shown in Figure 15, but the fibers are shorter. Probably, it is due to the reduction time in both steps of the synthesis and because the agitation in the equipment used for such a high quantity of material makes the orientation of the fibers difficult.

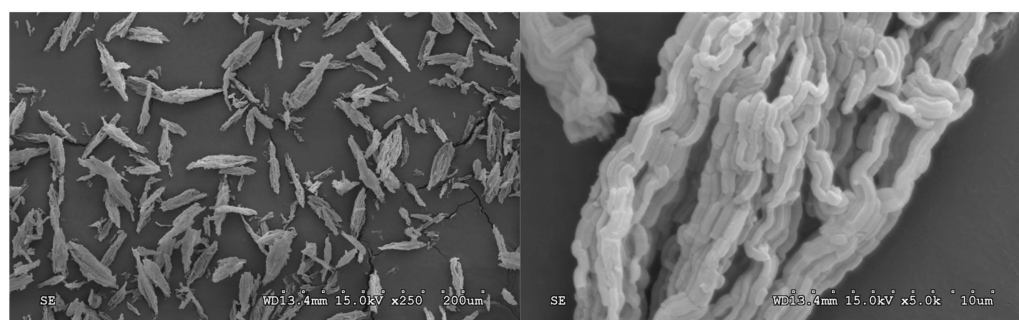


Figure 15. SEM micrographs of the synthesized SBA-15 in the scaling process.

The results obtained in the smoking tests are acceptable and very promising. The reduction capabilities presented are lower than those obtained when using TEOS as the silicate source [41,42] and also lower than those obtained with sodium silicate at lab scale, thus highlighting the need for a tuning of the scaling process.

3. Materials and Methods

3.1. Synthesis of Materials

Different stick-like morphology SBA-15s were synthesized in our laboratory according with the method described by Kosuge et al. [26] including some modifications. The first one was the inclusion of the hydrothermal treatment and the variation of the duration of this step. The second one was the study of the effect of the reaction (precipitation) time. Pluronic P123 was used as a surfactant and sodium silicate as the source of silicon; 3.7 g of Pluronic P123 from Sigma-Aldrich (Schnelldorf, Germany) were added in a solution of 127.8 g of HCl 2M (using HCl 11,32 M, from Merck). After mixing during 1 h, a solution of 7.84 g of sodium silicate, 1.37 g/cm³ density from Scharlau (Barcelona, Spain), dissolved in 74.72 mL of distilled water, was added. The solution was stirred at 30 °C during 24 h. Then, the hydrothermal treatment was carried out at 80 °C during different times, i.e., 0, 6, 15 and 24 h (samples H0, H6, H15 and H24, respectively). The white solid product obtained was collected by filtration, dried and then calcined at 550 °C in air during 5 h for removing the organic template. Additionally, several reaction times have been studied, 1/3, 2/3, 1, 2,

4, 6 and 24 h (samples R1/3, R2/3, R1, R4, R6 and R24, respectively). All these samples were hydrothermally treated at 80 °C during 24 h.

The scaling process was carried out in a 500 L reactor that allows obtaining up to 4 kg of SBA-15. The reactor has submersible heating elements and is thermally insulated. The temperature is controlled with a PID controller. The synthesis process was similar to that described for the laboratory scale. To carry out the hydrothermal treatment stage, the excess of the mother liquor was removed by filtration and the product was transferred to polypropylene containers. Finally, the SBA-15 was washed, filtered, dried and calcined. Scaling up was developed at 35 °C during 6 h at the reaction step and 80 °C during 15 h for the hydrothermal treatment.

3.2. Catalyst Characterization

A JEOL JSM-840 (Tokio, Japan) scanning electron microscope was used to obtain SEM micrographs operating at 15 kV, after covering the samples with gold employing a metallizer (Au)/evaporator (C) BALZERS, SCD 004 model (Balzers, Liechtenstein). The textural properties were obtained from the N₂ adsorption isotherms at 77 K, measured in an automatic Quantachrome AUTOSORB-6. The isotherms were recorded and the surface area was obtained according to the BET method. The pore size distributions were obtained applying the BJH model with cylindrical geometry of the pores. The total volumes were determined from the N₂ adsorbed at $P/P_0 = 0.965$ and micropore volumes were calculated according to the Dubinin–Raduskevich equation. The X-ray diffraction (XRD) patterns were obtained using a Bruker CCD-Apex monocrystals XR diffractometer, which employed Ni-filtered CuK α radiation ($\lambda K\alpha = 0.15406$ nm), between 0.5 and 5° (2 θ) with a step size of 0.0131° and time step of 18.87 s. The unit cell parameter was calculated as $a_0 = \lambda/(\sqrt{3}\sin\theta)$. Apparent density was measured determining the volume occupied by a given mass of SBA-15.

3.3. Smoking Experiments

Reference tobacco 3R4F supplied by the Center for Tobacco Reference of Kentucky University was used in this study. Before performing the smoking experiments, 100–200 cigarettes were disassembled and the tobacco, the filter and the paper were weighed separately. The tobacco was mixed with the SBA-15 materials and the cigarettes were reassembled. Cigarettes were prepared mixing manually around 96% conditioned tobacco with 4 wt% catalyst. To promote the adhesion of the SBA-15 to the tobacco fibers, EtOH (Montplet, Barcelona, Spain) was added during mixing. Vigorous mixing was carried out manually until the fibers were well homogeneously covered with the SBA-15. Then, the cigarettes were conditioned for at least 48 h at 22 °C and a relative humidity of 60%.

Smoking experiments were performed as described elsewhere [41], following the ISO 3303 smoking regime. The gaseous fraction of tobacco smoke was collected in a Tedlar bag and analyzed by CG/TCD (CO and CO₂) and GC/FID FID (not condensed fraction) in an Agilent 6890N chromatograph with a GS-GASPRO column. The total particulate matter (TPM) condensed in the trap located before the Tedlar bag was extracted with isopropanol (Fisher Scientific, Madrid, Spain) following the ISO4387 standard and analyzed by GC/MS in an Agilent 6890N chromatograph with an HP-5-MS column. The identification of the different compounds was done by comparison with the Wiley MS library. In this work, 30 compounds were analyzed in the gaseous fraction collected in the Tedlar bag and 40 compounds were analyzed in the TPM. Synthesis experiments, materials characterization and smoking experiments were duplicated and results presented correspond to the average of the two runs. Reproducibility was different depending on the experiment and parameters determined and were within the usual range expected in this type of experiment.

4. Conclusions

The results obtained show that, despite obtaining a material with acceptable textural properties when eliminating the hydrothermal treatment, this stage is necessary to obtain good reductions in the compounds generated in the tobacco smoking process. Moreover, when the time of hydrothermal treatment increases, a more orderly material is obtained with lower apparent density. The reductions in the generated compounds in the smoking experiments when the synthesized compounds are mixed with tobacco fibers increase with the hydrothermal treatment time, reaching the best results at 24 h of treatment. For this application, reductions obtained present a positive correlation with the textural properties developed and a negative correlation with the apparent density. Apparent density appears as a useful complementary variable for understanding the correlation of the catalyst performance in smoking application and its textural properties.

Textural properties present a maximum with reaction time as well as the reductions obtained in the TPM, nicotine, CO and most families of compounds, both in the gas and liquid fractions. Short reaction times (20 min) are not enough to obtain adequate textural properties nor reductions in compounds generated in smoking experiments. Reaction times around 1–2 h yield materials with fully developed textural properties and the best performance in the tobacco smoking application.

For the first time on record, a system that allows obtaining SBA-15 of the order of kg (4 kg) has been carried out. Materials with textural properties and behaviors in the smoking process close to those at a laboratory scale can be obtained. These results constitute a very promising basis for the development of an industrial scale process. Optimizing the time and replacing the TEOS precursor usually employed in the synthesis of SBA-15 with sodium silicate, results in energy saving of the process, reducing cost and toxicity of the precursor, which makes the synthesis process more environmentally friendly.

Author Contributions: Conceptualization, N.J.-S. and A.M.; methodology, N.J.-S. and A.M.; validation, N.J.-S. and A.M.; investigation, N.J.-S. and I.M.-C.; data curation, N.J.-S. and I.B.; writing—original draft preparation, D.B.; writing—review and editing, N.J.-S., M.B. and A.M.; visualization, N.J.-S.; project administration, A.M.; funding acquisition, A.M. All authors have read and agreed to the published version of the manuscript.

Funding: This research was funded by the Spanish “Secretaría de Estado de Investigación” of the Ministerio de Ciencia e Innovación (CTQ2015-70726-P), Generalitat Valenciana (PROMETEO/2016/056, PROMETEO 2020/093 and IDIFEDER 2018/009).

Acknowledgments: Financial support for this investigation has been provided by the Spanish “Secretaría de Estado de Investigación” of the Ministerio de Ciencia e Innovación (CTQ2015-70726-P), Generalitat Valenciana (PROMETEO/2016/056, PROMETEO 2020/093 and IDIFEDER 2018/009).

Conflicts of Interest: The authors declare no conflict of interest.

References

1. Sing, K.S.W.; Everett, D.H.; Haul, R.A.W.; Moscou, L.; Pierotti, R.A.; Rouquerol, J.; Siemieniewska, T. Reporting Physisorption data for gas/solid systems with special reference to the determination of surface area and porosity. *Pure Appl. Chem.* **1985**, *57*, 603–619. [[CrossRef](#)]
2. Kresge, C.T.; Leonowicz, M.E.; Roth, W.; Vartuli, J.C.; Beck, J.S. Ordered mesoporous molecular sieves synthesized by a liquid-crystal template mechanism. *Nature* **1992**, *359*, 710–712. [[CrossRef](#)]
3. Zhao, D.; Feng, J.; Huo, Q.; Melosh, N.; Fredrickson, G.H.; Chmelka, B.F.; Stucky, G.D. Triblock copolymer syntheses of mesoporous silica with periodic 50 to 300 angstrom pores. *Science* **1998**, *279*, 548–552. [[CrossRef](#)] [[PubMed](#)]
4. Zhao, D.; Huo, Q.; Feng, J.; Chmelka, B.F.; Stucky, G.D. Nonionic Triblock and star diblock copolymer and oligomeric surfactant syntheses of highly ordered, hydrothermally stable, mesoporous silica structures. *J. Am. Chem. Soc.* **1998**, *120*, 6024–6036. [[CrossRef](#)]
5. Beck, J.S.; Vartuli, J.C.; Roth, W.; Leonowicz, M.E.; Kresge, C.T.; Schmitt, K.D.; Chu, C.T.W.; Olson, D.H.; Sheppard, E.W.; McCullen, S.B.; et al. A new family of mesoporous molecular sieves prepared with liquid crystal templates. *J. Am. Chem. Soc.* **1992**, *114*, 10834–10843. [[CrossRef](#)]
6. Marín-Lasheras, E.; Téllez-Arís, C. Síntesis de Materiales Mesoporosos Ordenados Silíceos con Cafeína Micelada Encapsulada. Master’s Thesis, Universidad de Zaragoza, Zaragoza, Spain, 2011.

7. Johansson, E.M. Controlling the Pore Size and Morphology of Mesoporous Silica. Licentiate Thesis, Linköping University, Linköping, Sweden, 2010.
8. Sierra, I.; Pérez-Quintanilla, D. Heavy metal complexation on hybrid mesoporous silicas: An approach to analytical applications. *Chem. Soc. Rev.* **2013**, *42*, 3792–3807. [[CrossRef](#)]
9. Boccardi, E.; Liverani, L.; Beltran, A.M.; Günther, R.; Schmidt, J.; Peukert, W.; Boccaccini, A.R. Mesoporous silica submicron particles (MCM-41) incorporating nanoscale Ag: Synthesis, characterization and application as drug delivery coatings. *J. Porous Mater.* **2019**, *26*, 443–453. [[CrossRef](#)]
10. Alamdari, A.; Karimzadeh, R. Faradaic number as a criterion for the promotion effect of external electric field on the heterogeneous oxidative cracking of liquefied petroleum gas on ZSM-5 supported catalyst. *React. Kinet. Mech. Catal.* **2018**, *123*, 723–742. [[CrossRef](#)]
11. Eguílaz, M.; Villalonga, R.; Rivas, G. Electrochemical biointerfaces based on carbon nanotubes-mesoporous silica hybrid material: Bioelectrocatalysis of hemoglobin and biosensing applications. *Biosens. Bioelectron.* **2018**, *111*, 144–151. [[CrossRef](#)]
12. Hou, Q.; Lin, W.G.; Wei, F.; Yang, J.Y.; Zhu, J.H. Utilizing acid immersion to elevate the performance of zeolite in liquid adsorption of N'-nitrosornicotine (NNN). *Solid State Sci.* **2013**, *16*, 143–151. [[CrossRef](#)]
13. Nguyen, Q.N.K.; Yen, N.T.; Hau, N.D.; Tran, H.L. Synthesis and characterization of mesoporous silica SBA-15 and ZnO/SBA-15 photocatalytic materials from the ash of brickyards. *J. Chem.* **2020**, *2020*. [[CrossRef](#)]
14. Niculescu, V.; Aldea, N.; Rednic, V.; Parvulescu, V. Platinum mesoporous silica catalysts for liquid media oxidation. *Anal. Lett.* **2019**, *52*, 5–19. [[CrossRef](#)]
15. Fulvio, P.F.; Pikus, S.; Jaroniec, M. Tailoring properties of SBA-15 materials by controlling conditions of hydrothermal synthesis. *J. Mater. Chem.* **2005**, *15*, 5049–5053. [[CrossRef](#)]
16. Zhao, D.; Sun, J.; Li, Q.; Stucky, G.D. Morphological control of highly ordered mesoporous silica SBA-15. *Chem. Mater.* **2000**, *12*, 275–279. [[CrossRef](#)]
17. Dong, X.; Wang, Y.; Dan, H.; Hong, Z.; Song, K.; Xian, Q.; Ding, Y. A facile route to synthesize mesoporous SBA-15 silica spheres from powder quartz. *Mater. Lett.* **2017**, *204*, 97–100. [[CrossRef](#)]
18. Carrero, A.; Moreno, J.; Aguado, J.; Calleja, G. Control of SBA-15 materials morphology by modification of synthesis conditions. *Stud. Surf. Sci. Catal.* **2008**, *174*, 321–324. [[CrossRef](#)]
19. Zhou, Y.-Y.; Li, X.-X.; Chen, Z.-X. Rapid synthesis of well-ordered mesoporous silica from sodium silicate. *Powder Technol.* **2012**, *226*, 239–245. [[CrossRef](#)]
20. Van Bavel, E.; Cool, P.; Aerts, K.; VanSant, E.F. Plugged hexagonal templated silica (PHTS): An in-depth study of the structural characteristics. *J. Phys. Chem. B* **2004**, *108*, 5263–5268. [[CrossRef](#)]
21. Galarneau, A.; Cambon, H.; Di Renzo, F.; Ryoo, R.; Choi, M.; Fajula, F. Microporosity and connections between pores in SBA-15 mesostructured silicas as a function of the temperature of synthesis. *New J. Chem.* **2003**, *27*, 73–79. [[CrossRef](#)]
22. Benamor, T.; Vidal, L.; Lebeau, B.; Marichal, C. Influence of synthesis parameters on the physico-chemical characteristics of SBA-15 type ordered mesoporous silica. *Microporous Mesoporous Mater.* **2012**, *153*, 100–114. [[CrossRef](#)]
23. Guillet-Nicolas, R.; Bérubé, F.; Thommes, M.; Janicke, M.T.; Kleitz, F. Selectively tuned pore condensation and hysteresis behavior in mesoporous SBA-15 silica: Correlating material synthesis to advanced gas adsorption analysis. *J. Phys. Chem. C* **2017**, *121*, 24505–24526. [[CrossRef](#)]
24. Liu, J.; Yang, Q.; Zhao, X.; Zhang, L. Pore size control of mesoporous silicas from mixtures of sodium silicate and TEOS. *Microporous Mesoporous Mater.* **2007**, *106*, 62–67. [[CrossRef](#)]
25. Rahmat, N.; Hamzah, F.; Sahiron, N.; Mazlan, M.; Zahari, M.M. Sodium silicate as source of silica for synthesis of mesoporous SBA-15. *IOP Conf. Ser. Mater. Sci. Eng.* **2016**, *133*, 012011. [[CrossRef](#)]
26. Kosuge, K.; Sato, T.; Kikukawa, A.N.; Takemori, M. Morphological control of rod- and fiberlike SBA-15 type mesoporous silica using water-soluble sodium silicate. *Chem. Mater.* **2004**, *16*, 899–905. [[CrossRef](#)]
27. Koh, M.H.; Azaman, S.A.H.; Hameed, B.H.; Din, A.T.M. Surface morphology and physicochemical properties of ordered mesoporous silica SBA-15 synthesized at low temperature. *IOP Conf. Ser. Mater. Sci. Eng.* **2017**, *206*, 012056. [[CrossRef](#)]
28. Marcilla, A.; Siurana, A.G.; Berenguer, D.; Martínez-Castellanos, I.; Beltrán, M. Reduction of tobacco smoke components yield in commercial cigarette brands by addition of HUSY, NaY and Al-MCM-41 to the cigarette rod. *Toxicol. Rep.* **2015**, *2*, 152–164. [[CrossRef](#)]
29. Zhou, Y.; Gao, L.; Gu, F.; Yang, J.Y.; Yang, J.; Wei, F.; Wang, Y.; Zhu, J.H. Functional mesoporous material derived from 3D net-linked SBA-15. *Chem. A Eur. J.* **2009**, *15*, 6748–6757. [[CrossRef](#)]
30. Xu, Y.; Zhu, J.H.; Ma, L.L.; Ji, A.; Wei, Y.L.; Shang, X.Y. Removing nitrosamines from mainstream smoke of cigarettes by zeolites. *Microporous Mesoporous Mater.* **2003**, *60*, 125–138. [[CrossRef](#)]
31. Meier, W.; Siegmann, K. Significant reduction of carcinogenic compounds in tobacco smoke by the use of zeolite catalysts. *Microporous Mesoporous Mater.* **1999**, *33*, 307–310. [[CrossRef](#)]
32. Marcilla, A.; Beltrán, M.I.; Siurana, A.G.; Martínez, I.; Berenguer, D. Effect of the concentration of siliceous materials Added to tobacco cigarettes on the composition of the smoke generated during smoking. *Ind. Eng. Chem. Res.* **2015**, *54*, 1916–1929. [[CrossRef](#)]

33. Shi, C.L.; Li, S.H.; Sun, X.D.; Wang, Z.P.; Wang, Y.-Z.; Xiong, J.-W.; Gu, W.-B.; Wang, W.-M.; Yao, H.-M.; Wang, Y.; et al. New activated carbon sorbent with the zeolite-like selectivity to capture tobacco-specific nitrosamines in solution. *Chem. Eng. J.* **2018**, *339*, 170–179. [[CrossRef](#)]
34. Marcilla, A.; Siurana, A.G.; Berenguer, D.; Martínez-Castellanos, I.; Beltrán, M. Reduction of tobacco smoke components yields by zeolites and synthesized Al-MCM-41. *Microporous Mesoporous Mater.* **2012**, *161*, 14–24. [[CrossRef](#)]
35. Li, Y.Y.; Wan, M.M.; Zhu, J.H. Cleaning carcinogenic nitrosamines with zeolites. *Environ. Chem. Lett.* **2014**, *12*, 139–152. [[CrossRef](#)]
36. Yong, G.-P.; Jin, Z.-X.; Tong, H.-W.; Yan, X.-Y.; Li, G.-S.; Liu, S.-M. Selective reduction of bulky polycyclic aromatic hydrocarbons from mainstream smoke of cigarettes by mesoporous materials. *Microporous Mesoporous Mater.* **2006**, *91*, 238–243. [[CrossRef](#)]
37. Lin, W.G.; Zhou, Y.; Cao, Y.; Zhou, S.L.; Wan, M.M.; Wang, Y.; Zhu, J.H. Applying heterogeneous catalysis to health care: In situ elimination of tobacco-specific nitrosamines (TSNAs) in smoke by molecular sieves. *Catal. Today* **2013**, 52–61. [[CrossRef](#)]
38. Marcilla, A.; Beltrán, M.I.; Gómez-Siurana, A.; Berenguer, D.; Martínez-Castellanos, I. Nicotine/mesoporous solids interactions at increasing temperatures under inert and air environments. *J. Anal. Appl. Pyrolysis* **2016**, *119*, 162–172. [[CrossRef](#)]
39. Calabuig, E.; Juárez-Serrano, N.; Marcilla, A. TG-FTIR study of evolved gas in the decomposition of different types of tobacco. Effect of the addition of SBA-15. *Thermochimica Acta.* **2019**, *671*, 209–219. [[CrossRef](#)]
40. Gomis, A.M.; Gómez-Siurana, A.; Muñoz, D.B.; Martínez-Castellanos, I.; Beltrán, M. Effect of mesoporous catalysts on the mainstream tobacco smoke of 3R4F and 1R5F reference cigarettes. *Am. J. Chem. Eng.* **2015**, *3*, 1. [[CrossRef](#)]
41. Juárez-Serrano, N.; Asensio, J.; Martínez-Castellanos, I.; Beltrán, M.; Marcilla, A. The effect of temperature and time of the hydrothermal treatment in the sba-15 synthesis process on the structure and textural properties and the ability to reduce the evolution of tars in tobacco smoking. *Catalysts* **2020**, *10*, 272. [[CrossRef](#)]
42. Juárez-Serrano, N.; Asensio, J.; Blasco, I.; Beltrán, M.; Marcilla, A. Effect of time, temperature and stirring rate used in the first step of the synthesis of SBA-15 on its application as reductor of tars in tobacco smoke. *Catalysts* **2021**, *11*, 375. [[CrossRef](#)]
43. Tkachenko, O.P.; Klementiev, K.V.; Löffler, E.; Ritzkopf, I.; Schuth, F.; Bandyopadhyay, M.; Grabowski, S.; Gies, H.; Hagen, V.; Muhler, M.; et al. The structure of zinc and copper oxide species hosted in porous siliceous matrices. *Phys. Chem. Chem. Phys.* **2003**, *5*, 4325–4334. [[CrossRef](#)]
44. Thielemann, J.P.; Girgsdies, F.; Schlögl, R.; Hess, C. Pore structure and surface area of silica SBA-15: Influence of washing and scale-up. *Beilstein J. Nanotechnol.* **2011**, *2*, 110–118. [[CrossRef](#)]
45. Rodríguez-Reinoso, F. Problemas más habituales en el uso de la adsorción física como técnica de caracterización de sólidos porosos. *Rev. Grupo Espec. Adsorción RSEQ* **2010**, *0*, 5–16.
46. Sing, K.S.; Williams, R.T. Physisorption hysteresis loops and the characterization of nanoporous materials. *Adsorpt. Sci. Technol.* **2004**, *22*, 773–782. [[CrossRef](#)]
47. Nagata, H.; Takimura, M.; Yamasaki, Y.; Nakahira, A. syntheses and characterization of bulky mesoporous silica MCM-41 by hydrothermal hot-pressing method. *Mater. Trans.* **2006**, *47*, 2103–2105. [[CrossRef](#)]
48. Dhaneswara, D.; Fatriansyah, J.F.; Putranto, D.A.; Utami, S.A.A.; Delayori, F. The structure heterogeneity of silica mesopores of Sba-15 in respect to the pluronic 123 template concentration. In *IOP Conference Series: Material Science and Engineering*; Institute of Physics Publishing: Bristol, UK, 2018; Volume 285, p. 12032. [[CrossRef](#)]
49. Colilla, M.; Balas, F.; Manzano, M.; Vallet-Regí, M. Novel method to enlarge the surface area of SBA-15. *Chem. Mater.* **2007**, *19*, 3099–3101. [[CrossRef](#)]
50. Klimova, T.; Esquivel, A.; Reyes, J.; Rubio, M.; Bokhimi, X.; Aracil, J. Factorial design for the evaluation of the influence of synthesis parameters upon the textural and structural properties of SBA-15 ordered materials. *Microporous Mesoporous Mater.* **2006**, *93*, 331–343. [[CrossRef](#)]
51. Van Der Voort, P.; Ravikovitch, P.I.; De Jong, K.P.; Benjelloun, M.; Van Bavel, E.; Janssen, A.H.; Neimark, A.V.; Weckhuysen, B.M.; Vansant, E.F. A new templated ordered structure with combined micro- and mesopores and internal silica nanocapsules. *J. Phys. Chem. B* **2002**, *106*, 5873–5877. [[CrossRef](#)]